ADVANCED FUNCTIONAL MATERIALS
www.afm-journal.de

A Self-Standing and Flexible Electrode of $Li_4Ti_5O_{12}$ Nanosheets with a N-Doped Carbon Coating for High Rate Lithium Ion Batteries

Na Li, Guangmin Zhou, Feng Li, Lei Wen, and Hui-Ming Cheng**

Flexible energy-storage devices have attracted growing attention with the fast development of bendable electronic systems. Thus, the search for reliable electrodes with both high mechanical flexibility and excellent electron and lithium-ion conductivity has become an urgent task. Carbon-coated nanostructures of $Li_4Ti_5O_{12}$ (LTO) have important applications in high-performance lithium ion batteries (LIBs). However, these materials still need to be mixed with a binder and carbon black and pressed onto metal substrates or, alternatively, by be deposited onto a conductive substrate before they are assembled into batteries, which makes the batteries less flexible and have a low energy density. Herein, a simple and scalable process to fabricate LTO nanosheets with a N-doped carbon coating is reported. This can be assembled into a film which can be used as a binder-free and flexible electrode for LIBs that does not require any current collectors. Such a flexible electrode has a long life. More significantly, it exhibits an excellent rate capability due to the thin carbon coating and porous nanosheet structures, which produces a highly conductive pathway for electrons and fast transport channels for lithium ions.

1. Introduction

Flexible electronics is an emerging and promising technology for the next-generation electronic devices such as roll-up displays, smart electronics, and wearable devices. To meet the needs for the future portable electronic industry, the development of flexible, lightweight and environmentally-friendly energy storage devices, in which electrodes are key components, are required.[1–8] Though several kinds of flexible composite electrodes have been reported,[9–15] it is still a great challenge to fabricate highly flexible energy storage devices with high energy and power densities, and excellent cyclic stability, while maintaining low cost. Searching for high performance flexible electrodes is thus becoming one of the key issues.

Spinel $Li_4Ti_5O_{12}$ (LTO) has attracted significant attention in the past few years as a suitable anode material for lithium ion batteries (LIBs) because of its outstanding ability to tolerate abuse and its excellent cycle life.[16–21] LTO exhibits an extremely flat charge/discharge plateau at 1.55 V vs. Li/Li^+, which is above the potential range where most types of electrolytes or solvents are reduced.[22–24] It can accommodate up to three lithium ions per molecule without volume change as a zero-strain insertion material.[25,26] These features make LTO a promising candidate for the anode of LIBs. However, the main disadvantage that restricts the use of LTO is its low electronic conductivity and moderate Li^+ diffusion coefficient.[27–30] To address the above issues, various nano/microstructured LTO materials have been synthesized for use as high performance anodes.[31,32] Among the nanostructures, nanosheets have been evaluated in an attempt to achieve a shorter transport distance for both lithium ions and electrons. However, the synthesis of ultrathin LTO nanosheets is quite challenging. To the best of our knowledge, all available LTO sheets show a thickness larger than 10 nm.[33,34]

Another strategy for improving the electrochemical performance involves carbon coating the LTO materials, which can improve the electron transfer through the interface of the electrode material particles and suppress the interfacial reaction.[35–40] Carbon-coated spinel LTO nanostructures have attained more than 90% of the theoretical capacity and exhibited excellent rate capability.[31,35,36] However, these carbon-coated LTO nanostructures still need to be mixed with a binder and conductive additive such as carbon black and pressed onto a metal substrate as a current collector or, alternatively, deposited onto a conductive substrate before they are assembled into batteries, which makes the batteries have poor flexibility and a low energy density. Therefore, it is expected that advancement in LIB technology can be achieved by combining both a flexible design approach and carbon-coated nanostructures, leading to a superior rate performance. By using flexible current collectors such as carbon nanotubes and fibers, flexible LTO composite electrodes have been obtained.[41,42] However only moderate charge/discharge rates have been achieved. Recently, we have

N. Li, G. Zhou, Prof. F. Li, Prof. L. Wen,
Prof. H.-M. Cheng,
Shenyang National Laboratory for Materials Science
Institute of Metal Research
Chinese Academy of Sciences
72 Wenhua RD, Shenyang 110016, China
E-mail: fli@imr.ac.cn; cheng@imr.ac.cn
N. Li
Department of Materials Science & Engineering
School of Chemistry and Materials Science
University of Science and Technology of China
Hefei 230026, China

DOI: 10.1002/adfm.201300495

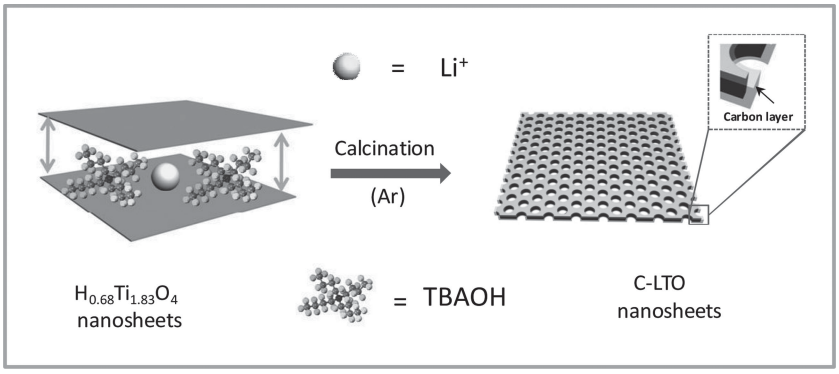

Figure 1. Schematic for the fabrication of C-LTO nanosheets.

developed a flexible LTO/graphene foam electrode which simultaneously provides high charge/discharge rates, but its energy density needs to be increased.[43]

In this work, we report a simple and scalable process to fabricate LTO nanosheets with N-doped carbon coating (denoted C-LTO nanosheets). Using this material, we developed a flexible film which can be directly used as a flexible electrode for LIBs. This flexible electrode shows an excellent rate capability and a significantly improved cycling performance.

2. Results and Discussion

2.1. Fabrication and Characterization of C-LTO Nanosheets

The schematic shown in **Figure 1** illustrates the synthesis of C-LTO nanosheets. Hydrous lithium titanate nanosheets were formed by the chemical lithiation of $H_{0.68}Ti_{1.83}O_4$ nanosheets in a LiOH solution. An annealing treatment in argon is used to convert the precursor into LTO nanosheets with N-doped carbon coating. Tetrabutylammonium hydroxide (TBAOH) was used as a carbon and nitrogen source to form a thin N-doped carbon layer on the surface of the LTO nanosheets. According to the thermogravimetric (TG) result (Figure S1, Supporting Information), the percentage of pyrolytic carbon in C-LTO nanosheets was 4 wt%. The morphology and microstructure of the C-LTO nanosheets were investigated using scanning electron microscopy (SEM) and transmission electron microscopy (TEM), as shown in **Figure 2**. Representative nanosheets appear to be loose and soft agglomerates with a size of tens of micrometers (Figure 2a). The low-magnification TEM image in Figure 2b shows that the LTO sheets are quite similar in appearance to graphene. In this image, the light regions suggest planar or curled thin sheets lying on the substrate, with an edge length more than 400 nm. Figure 2c reveals that the LTO nanosheets really have a porous structure composed of small nanoparticles instead of single-crystal. Between the small crystals, wormhole-like pores were formed and provide a large volume for electrolyte storage and ensure Li^+ diffusion in channels across the LTO nanosheet film anode. This provides remarkable rate capability and cycling performance. From the HRTEM image in Figure 2d, it can be observed that a thin uniform amorphous carbon layer is formed on the surface. A lattice spacing of 0.48 nm was observed, in good agreement with the d-spacing of 0.484 nm associated with the (111) direction of spinel LTO.

Atomic force microscopy (AFM) analyses (Figure 2e,f) display the 2D features of C-LTO nanosheets with a thickness of ≈2.5 nm. X-ray diffraction (XRD) patterns (**Figure 3**a) reveal that the $H_{0.68}Ti_{1.83}O_4$ nanosheets completely convert to spinel LTO after chemical lithiation and post-annealing. The Raman spectrum of the C-LTO nanosheets shows two bands at 1350 and 1590 cm^{-1}, which correspond to the D and G bands of carbon, respectively (Figure S2, Supporting Information). The specific surface area of the C-LTO nanosheets is 256 m^2 g^{-1} (Figure 3b). The high surface area is the result of not only the nanosheet structure but also the presence of inner nanopores. A narrow peak in pore size distribution indicates that the main pore size (inset in Figure 3b) in the C-LTO nanosheets is 4 nm, which confirms a uniform pore size distribution. A typical high-resolution XPS spectrum of N 1s for the C-LTO nanosheets is shown in Figure 3c. Peaks at binding energies of 398.5 and 400.5 eV can be attributed to pyridinic-N (C–N bond) and graphitic-N (C = N bond), respectively.[44] Furthermore, an additional peak at ca. 396 eV

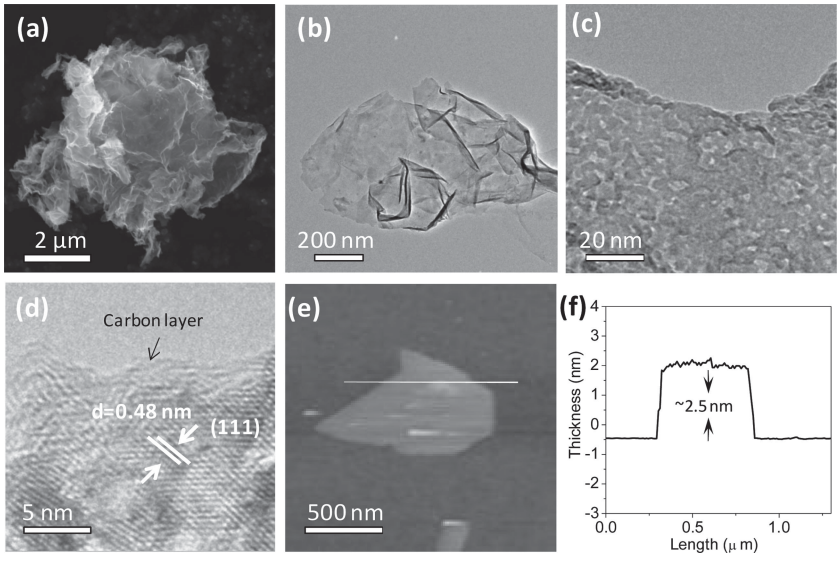

Figure 2. a) SEM image of C-LTO nanosheets. b) TEM image and c) high magnification TEM image of C-LTO nanosheets and d) HRTEM image of a C-LTO nanosheet with a nanoporous interior showing lattice fringes with a spacing of 0.48 nm. e) Representative AFM image and f) its corresponding thickness analysis taken along the white line in (e), which reveals a thickness of about 2.5 nm for C-LTO nanosheets.

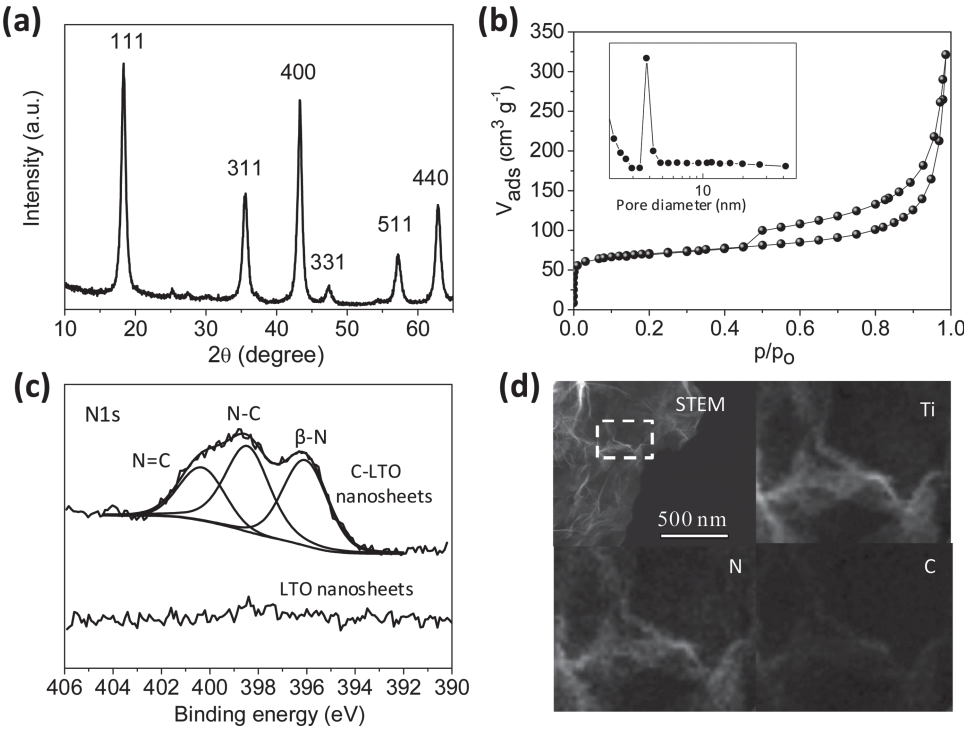

Figure 3. a) XRD pattern and b) N_2 adsorption/desorption isotherm (inset: pore size distribution) of C-LTO nanosheets. c) High resolution XPS spectra of N 1s in C-LTO nanosheets and LTO nanosheets. d) STEM image of C-LTO nanosheets and Ti, C and N element mapping of the square region.

was observed in the N 1s spectrum, which can be assigned to atomic β-N,[45] namely the substitution of O with N. High-angle annular dark-field STEM elemental mapping in Figure 3d confirms the homogeneous distribution of C and N on/inside the nanosheets.

2.2. Fabrication and Characterization of C-LTO Nanosheets Electrode

Self-standing C-LTO nanosheet films were prepared by assembling the C-LTO nanosheets by a vacuum filtration process (Figure S3, Supporting Information). The film electrodes have a robust mechanical stability because of the flexible nanosheet building blocks, which is similar to a piece of graphene paper.[46,47] Notably, the electrode is flexible (**Figure 4**a), and can be bent into arbitrary shapes. SEM images (Figure 4b–d) reveal that it has a uniform thickness (≈70 μm) throughout its cross-section, and the LTO nanosheets align parallel to form a layered structure. The porous nanosheet structure of this electrode provides a large specific volume for the fast transfer of Li^+. The electrical conductivity is significantly improved by the thin N-doped carbon coating on the surface. In the N-doped carbon, N-doping can enhance the reactivity and electronic conductivity.[48] Moreover, this unique electrode is a monolithic block. All of these factors contribute to the effective ambipolar diffusion of Li^+ and electrons into/out of LTO in the C-LTO nanosheet film electrode enabling remarkable rate capability and cycling performance.

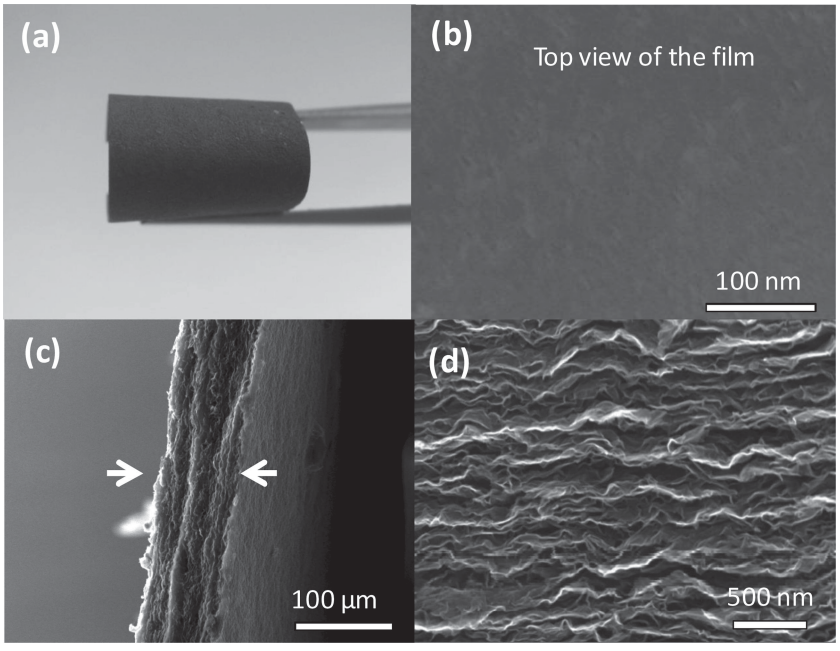

Figure 4. a) Photograph of a self-standing C-LTO nanosheet film electrode being bent, showing its good flexibility. b) Top view SEM image of a C-LTO nanosheet film electrode. c) Cross-section SEM image and d) high magnification image of a C-LTO nanosheet film electrode.

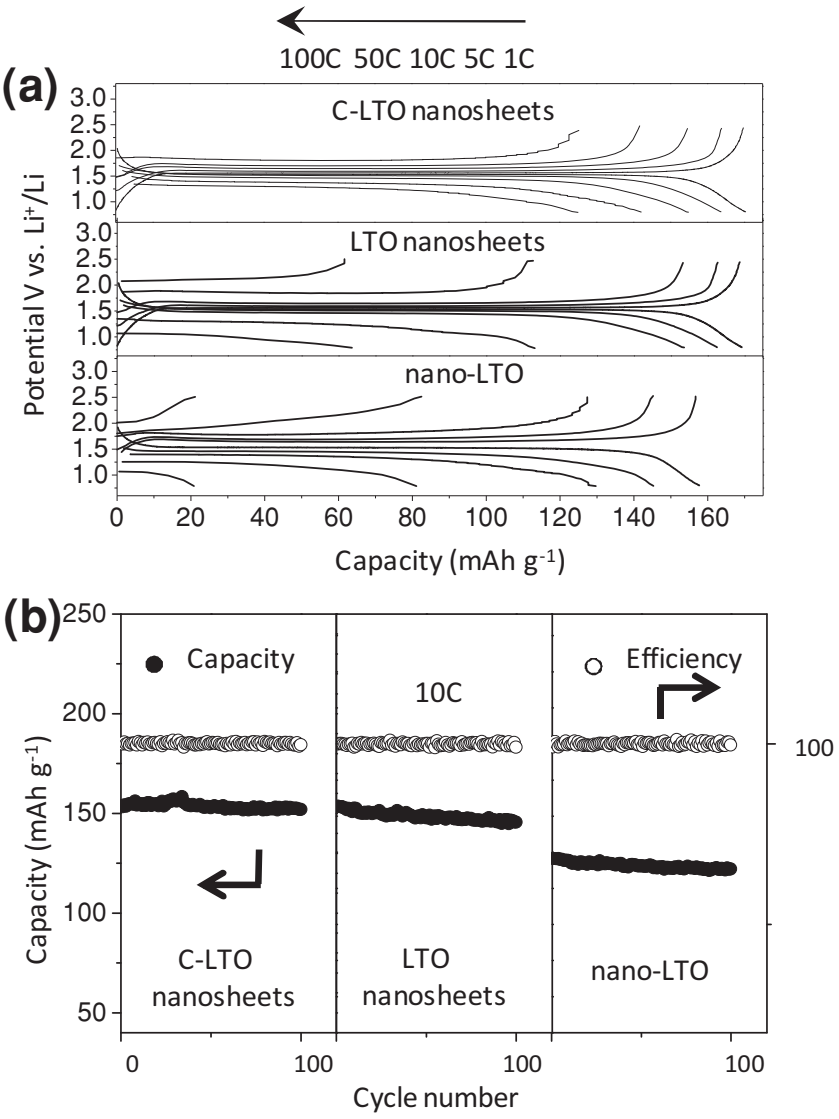

Figure 5. a) Galvanostatic discharge/charge voltage profiles cycled at different rates. b) Cycling performance at 10 C of the C-LTO nanosheet, LTO nanosheet film electrodes and nano-LTO electrode.

2.3. Electrochemical Performance of C-LTO Nanosheets Electrode

Electrochemical studies of the electrode were conducted using two-electrode cells with lithium metal as a counter electrode. The C-LTO nanosheet film electrode features a gravimetric capacity of 170 mAh g^{-1} at a rate of 1 C and can deliver up to 72% of the theoretical capacity at a high rate of 100 C (corresponding to 36 s charge/discharge) without deterioration over 100 cycles (**Figure 5**a). Moreover, the discharge curve of the electrode at high rates (up to 100 C) shows a long flat potential plateau, which ensures a constant power output, a very important factor for LIBs.[49] Although there is only 4.0 wt% N-doped carbon in the electrode and no ancillary materials, the rate performance of the electrode is much better than that of nanoporous LTO,[35] carbon-coated LTO,[28] TiN-coated LTO,[50] rutile-TiO_2-LTO,[34] LTO-graphene and LTO-carbon nanotube composites.[19,51] The performance of the C-LTO nanosheet thin film electrode could be attributed to the following two factors. First, the porous nanosheet structure possesses a large specific volume that facilitates the fast transfer of Li^+. Second, the electronic conductivity of the electrode is significantly improved by the thin N-doped carbon layer on the nanosheet surface, which ensures all the nanosheets have an ultrafast rate of electrochemical reaction.

For comparison, we also performed electrochemical experiments for LTO nanosheet film electrodes without N-doped carbon layer (Figure S4, Suppoting Information) and nano-LTO (LTO particle size <20 nm, Figure S5, Supporting Information). Figure 5a shows the charge/discharge voltage profiles of the C-LTO nanosheet, LTO nanosheet film electrodes and nano-LTO cycled at various current rates from 1 to 100 C. At a low discharge/charge current rate of <10 C, the capacities of the C-LTO nanosheet and LTO nanosheet film electrodes are comparable, which is in good agreement with the very recent reports that carbon-free LTO electrodes have shown excellent electrochemical performance without any conductive additives.[52,53] However, the C-LTO nanosheet film electrode delivers a discharge capacity of 131 mAh g^{-1} at a high rate of 100 C, which is 77% of the specific capacity at 1 C (**Figure 6**a). In contrast, the discharge capacity of the LTO nanosheet film electrode at the current rate of 100 C is 32% of the specific capacity at 1 C. The higher rate capability of the C-LTO nanosheet film electrode demonstrates that the N-doped carbon layer improves the high rate performance of LTO at discharge/charge current rates of >10 C. It is remarkable that the LTO nanosheet film electrode without a carbon layer exhibits a higher rate performance than that of nano-LTO. Another excellent property of the C-LTO nanosheet film electrode is its superior cycling performance with very slight capacity decay. After 100 discharge/charge cycles at 10 C, the C-LTO nanosheet film electrode delivers a specific capacity as high as 152 mAh g^{-1} (Figure 5b). Note that the capacity decreases less than 1% of the initial value after 100 cycles, demonstrating the excellent electrochemical stability of this self-standing flexible electrode. TEM images of the C-LTO nanosheet film electrode after 100 charge/discharge cycles at 10 C show that the nanosheet structure and nanoporous internal structure remained intact (Figure S6, Supporting Information).

The thin N-doped carbon layer on the nanosheet surface contributes to the good conductivity of the C-LTO nanosheets, which directly correlates to the excellent electrochemical performance and is confirmed by electrochemical impedance spectroscopy measurements. These cells were measured after the first cycle at a current rate of 1C in the charged state (2.5 V vs Li^+/Li) (Figure S7,

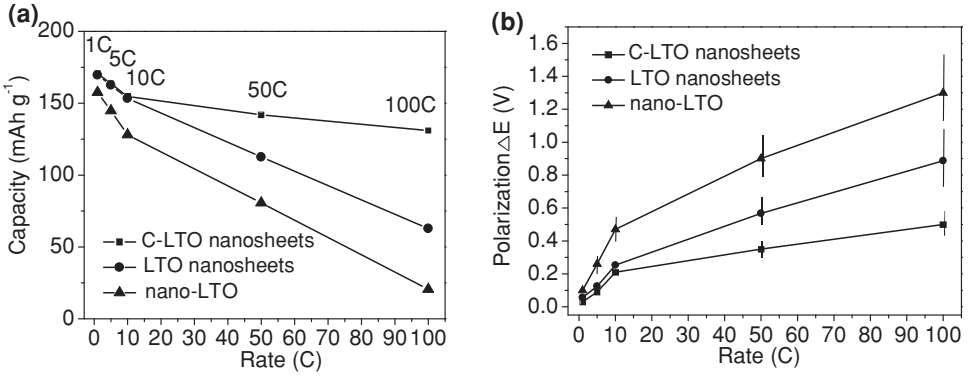

Figure 6. Electrochemical performance of the C-LTO nanosheet, LTO nanosheet film electrodes and nano-LTO electrode: a) rate capability, b) plots of ΔE versus C rates.

Supporting Information). The elements in the equivalent circuit include ohmic resistance of the electrolyte and cell components (Re), and charge-transfer resistance at the interface between the electrode and electrolyte (Rct).[54] The parameter Rct for the C-LTO nanosheets electrode (98.6 Ω) is much lower than that of the LTO nanosheets (155.4 Ω) and nano-LTO electrode (209.5 Ω), which means that the C-LTO nanosheet electrode has faster charge transfer than the others. Figure 6b shows the polarization of ΔE versus rate plots of the C-LTO nanosheet, LTO nanosheet film electrodes and the nano-LTO electrode. The value of ΔE is defined as the difference between the potentials of the charge and discharge plateaus. We can observe an increase of ΔE as a function of C-rate. This behavior is certainly due to the poor ionic conductivity of the electrode materials which limits the diffusion of the lithium ions. Both plots show dependence on the discharge/charge rates, while the ΔE of the C-LTO nanosheet film electrode is much smaller than that of the LTO nanosheet film electrode and nano-LTO electrode, suggesting a better rate capability.

3. Conclusions

LTO nanosheets were fabricated by a simple and scalable process. They consist of a nanoporous interior and a N-doped carbon-coated surface. The C-LTO nanosheets are assembled by vacuum filtration into yield mechanically robust self-standing films of ≈70 μm thickness. When the flexible LTO film was tested as a self-standing LIB anode, it showed an excellent rate performance and a good cycling stability derived from the thin uniform carbon layer and the porous structure, producing a highly conductive pathway for electrons and fast transport channels for lithium ions. The self-standing LTO electrodes without any ancillary materials could open up new opportunities for LTO to power flexible electronic devices.

4. Experimental Section

4.1. Sample Preparation

Synthesis of C-LTO Nanosheets: A titanate precursor of $H_{0.68}Ti_{1.83}O_4$ was prepared according to a procedure previously reported.[55] $H_{0.68}Ti_{1.83}O_4$ (1.2 g) was dispersed in a TBAOH solution (300 mL, 0.2 mol L^{-1}) and was shaken for 7 days at room temperature until it is exfoliated to a white colloidal suspension of $H_{0.68}Ti_{1.83}O_4$ nanosheets.[56] Lithium hydroxide ($LiOH{\cdot}H_2O$, 63 mg) was added to the above solution (50 mL) at ambient temperature under magnetic stirring (10 min) and the mixture was freeze-dried to form a white powder. Finally, the white powder was heated at 600 °C for 6 h under an argon atmosphere. After heat treatment, the color of the initial white powder changed to dark gray. Here, TBAOH was used as the carbon and nitrogen source to form thin N-doped carbon coating on the surface of the LTO nanosheets.

Synthesis of LTO Nanosheets: When the above white powder was heated at 600 °C for 6 h under an air atmosphere, LTO nanosheets without N-doped carbon coating layer were obtained.

Synthesis of Flexible C-LTO Nanosheet Film Electrode: The C-LTO nanosheets were dispersed in *N*-methylpyrolidone (NMP) at a concentration of 25 mg L^{-1}, and were sonicated for 10 h to enhance the dispersion. A self-standing film was synthesized by vacuum-filtration on a Whatman polycarbonate track-etched membrane (0.2 mm in pore diameter), which results in an interwoven and mechanically robust LTO nanosheet film attached to the membrane. Then a self-standing electrode was obtained by removing the air-dried LTO nanosheet film and further dried for 12 h at 70 °C in air, and then cut or punched to the desired size. The typical thickness of the C-LTO nanosheet film electrode was ≈70 μm.

Synthesis of Flexible LTO Nanosheet Film Electrode: The procedure was the same as that for the C-LTO nanosheet film electrode except for using LTO nanosheets.

Synthesis of LTO Nanoparticles (Nano-LTO): Nano-LTO was prepared according to a procedure previously reported.[57]

4.2. Characterization

XRD patterns of samples were recorded on a Rigaku diffractometer using Cu Kα irradiation. SEM, TEM and AFM images were obtained on a Nova NanoSEM 430 at 15 kV, Tecnai F20 at 200 kV and Veeco MultiMode/NanoScope IIIa, respectively. High-angle annular dark-field STEM mapping was carried out using a Tecnai F30 TEM with an accelerating voltage of 300 kV. TG measurements were carried out on a Netzsch-STA 449C from 30 to 1000 °C at a heating rate of 10 °C min^{-1} in air. The specific surface areas were determined by a Micromeritics ASAP 2010M, and pore size distribution was determined from the desorption branch of the isotherm using the DFT model. Raman spectra were collected using a 632.8 nm laser with JY HR800.

4.3. Electrochemical Measurements

For electrochemical measurements of the self-standing C-LTO nanosheet and LTO nanosheet film electrodes, coin cells were used. In both cases, a lithium metal foil was used as a counter electrode,

1 M $LiPF_6$ in ethylene carbonate and dimethyl carbonate (1:1 vol) as electrolyte, and a polypropylene film (Celgard 2400) as a separator. The electrochemical performance was measured at different rates at room temperature. All tests on the self-standing C-LTO nanosheet and LTO nanosheet film electrodes were performed without current collectors, carbon black conducting additives and binders. A reference nano-LTO electrode was prepared by mixing the nano-LTO, carbon black (Super-P) and poly(vinyl difluoride) at a weight ratio of 80:10:10. Cells were assembled in an argon-filled glove-box with oxygen and water contents below 1 and 0.1 ppm, respectively. All the capacities and C-rate currents were calculated based on the LTO active materials (1C corresponding to 175 mA g^{-1}).

Supporting Information

Supporting Information is available from the Wiley Online Library or from the author.

Acknowledgements

This work was supported by Ministry of Science and Technology of China (No. 2011CB932604) and National Science Foundation of China (Nos. 50921004 and 51172239).

Received: February 6, 2013
Revised: March 13, 2013
Published online: May 16, 2013

[1] H. Nishide, K. Oyaizu, *Science* **2008**, *319*, 737.
[2] M. Armand, J. M. Tarascon, *Nature* **2008**, *451*, 652.
[3] Y. Yang, S. Jeong, L. B. Hu, H. Wu, S. W. Lee, Y. Cui, *Proc. Natl. Acad. Sci. USA* **2011**, *108*, 13013.
[4] K. T. Nam, D. W. Kim, P. J. Yoo, C. Y. Chiang, N. Meethong, P. T. Hammond, Y. M. Chiang, A. M. Belcher, *Science* **2006**, *312*, 885.
[5] L. Yang, S. Cheng, Y. Ding, X. B. Zhu, Z. L. Wang, M. L. Liu, *Nano Lett.* **2012**, *12*, 321.
[6] B. Scrosati, *Nat. Nanotechnol.* **2007**, *2*, 598.
[7] J. A. Rogers, T. Someya, Y. Huang, *Science* **2010**, *327*, 1603.
[8] M. H. Park, K. Kim, J. Kim, J. Cho, *Adv. Mater.* **2010**, *22*, 415.
[9] S. Luo, K. Wang, J. P. Wang, K. L. Jiang, Q. Q. Li, S. S. Fan, *Adv. Mater.* **2012**, *24*, 2294.
[10] Y. H. Kwon, S. W. Woo, H. R. Jung, H. K. Yu, K. Kim, B. H. Oh, S. Ahn, S. Y. Lee, S. W. Song, J. Cho, H. C. Shin, J. Y. Kim, *Adv. Mater.* **2012**, *24*, 5192.
[11] B. Zhang, Y. Yu, Z. D. Huang, Y. B. He, D. Jang, W. S. Yoon, Y. W. Mai, F. Y. Kang, J. K. Kim, *Energy Environ. Sci.* **2012**, *5*, 9895.
[12] X. L. Jia, C. Z. Yan, Z. Chen, R. R. Wang, Q. Zhang, L. Guo, F. Wei, Y. F. Lu, *Chem. Commun.* **2011**, *47*, 9669.
[13] H. Gwon, H. S. Kim, K. U. Lee, D. H. Seo, Y. C. Park, Y. S. Lee, B. T. Ahna, K. Kang, *Energy Environ. Sci.* **2011**, *4*, 1277.
[14] Z. Chen, D. Q. Zhang, X. L. Wang, X. L. Jia, F. Wei, H. X. Li, Y. F. Lu, *Adv. Mater.* **2012**, *24*, 2030.
[15] L. Jabbour, C. Gerbaldi, D. Chaussy, E. Zeno, S. Bodoardo, D. Beneventi, *J. Mater. Chem.* **2010**, *20*, 7344.
[16] E. Ferg, R. J. Gummow, A. Dekock, M. M. Thackeray, *J. Electrochem. Soc.* **1994**, *141*, L147.
[17] X. Lu, L. Zhao, X. He, R. Xiao, L. Gu, Y. S. Hu, H. Li, Z. Wang, X. Duan, L. Q. Chen, J. Maier, Y. Ikuhara, *Adv. Mater.* **2012**, *24*, 3233.
[18] W. J. H. Borghols, M. Wagemaker, U. Lafont, E. M. Kelder, F. M. Mulder, *J. Am. Chem. Soc.* **2009**, *131*, 17786.
[19] L. F. Shen, C. Z. Yuan, H. J. Luo, X. G. Zhang, K. Xu, F. Zhang, *J. Mater. Chem.* **2011**, *21*, 761.
[20] E. Kang, Y. S. Jung, G. H. Kim, J. Y. Chun, U. Wiesner, A. C. Dillon, J. K. Kim, J. Lee, *Adv. Funct. Mater.* **2011**, *21*, 4349.
[21] J. Kim, J. Cho, *Electrochem. Solid-State Lett.* **2007**, *10*, A81.
[22] G. G. Amatucci, F. Badway, A. D. Pasquier, T. Zheng, *J. Electrochem. Soc.* **2001**, *148*, A930.
[23] T. Ohzuku, A. Ueda, N. Yamamoto, *J. Electrochem. Soc.* **1995**, *142*, 1431.
[24] L. F. Shen, X. G. Zhang, H. S. Li, C. Z. Yuan, G. Z. Cao, *J. Phys. Chem. Lett.* **2011**, *2*, 3096.
[25] L. Aldon, P. Kubiak, M. Womes, J. C. Jumas, J. Olivier-Fourcade, J. L. Tirado, J. I. Corredor, C. P. Vicente, *Chem. Mater.* **2004**, *16*, 5721.
[26] J. Haetge, P. Hartmann, K. Brezesinski, J. Janek, T. Brezesinski, *Chem. Mater.* **2011**, *23*, 4384.
[27] L. F. Shen, C. Z. Yuan, H. J. Luo, X. G. Zhang, K. Xu, Y. Y. Xia, *J. Mater. Chem.* **2010**, *20*, 6998.
[28] G. N. Zhu, H. J. Liu, J. H. Zhuang, C. X. Wang, Y. G. Wang, Y. Y. Xia, *Energy Environ. Sci.* **2011**, *4*, 4016.
[29] L. F. Shen, E. Uchaker, C. Z. Yuan, P. Nie, M. Zhang, X. G. Zhang, G. Z. Cao, *ACS Appl. Mater. Interfaces* **2012**, *4*, 2985.
[30] G. Du, N. Sharma, V. K. Peterson, J. A. Kimpton, D. Jia, Z. Guo, *Adv. Funct. Mater.* **2011**, *21*, 3990.
[31] J. M. Feckl, K. Fominykh, M. Doblinger, D. Fattakhova-Rohlfing, T. Bein, *Angew. Chem. Int. Ed.* **2012**, *51*, 7459.
[32] L. F Shen, E. Uchaker, X. G. Zhang, G. Z. Cao, *Adv. Mater.* **2012**, *24*, 6502.
[33] J. Z. Chen, L. Yang, S. H. Fang, Y. F. Tang, *Electrochim. Acta* **2010**, *55*, 6596.
[34] Y. Q. Wang, L. Gu, Y. G. Guo, H. Li, X. Q. He, S. Tsukimoto, Y. Ikuhara, L. J. Wan, *J. Am. Chem. Soc.* **2012**, *134*, 7874.
[35] L. Zhao, Y. S. Hu, H. Li, Z. Wang, L. Q. Chen, *Adv. Mater.* **2011**, *23*, 1385.
[36] H. G. Jung, S. T. Myung, C. S. Yoon, S. B. Son, K. H. Oh, K. Amine, B. Scrosati, Y. K. Sun, *Energy Environ. Sci.* **2011**, *4*, 1345.
[37] H. G. Jung, M. W. Jang, J. Hassoun, Y. K. Sun, B. Scrosati B, *Nat. Commun.* **2011**, *2*, 516.
[38] Y. B. He, B. H. Li, M. Liu, C. Zhang, W. Lv, C. Yang, J. Li, H. D. Du, B. Zhang, Q. H. Yang, J. K. Kim, F. Y. Kang, *Sci. Rep.* **2012**, *2*, 903.
[39] B. H. Li, C. P. Han, Y. B. He, C. Yang, H. D. Du, Q. H. Yang, F. Y. Kang, *Energy Environ. Sci.* **2012**, *5*, 9595.
[40] Y. B. He, F. Ning, B. Li, Q. S. Song, W. Lv, H. Dua, D. Zhai, F. Su, Q. H. Yang, F. Y. Kang, *J. Power Sources* **2012**, *202*, 253.
[41] L. B. Hu, H. Wu, F. La Mantia, Y. Yang, Y. Cui, *ACS Nano* **2010**, *4*, 5843.
[42] Y. Liu, S. Gorgutsa, C. Santato, M. Skorobogatiy, *J. Electrochem. Soc.* **2012**, *159*, A349.
[43] N. Li, Z. P. Chen, W. C. Ren, F. Li, H. M. Cheng, *Proc. Natl. Acad. Sci. USA* **2012**, *109*, 17360.
[44] S. Bhattacharyya, C. Cardinaud, G. Turban, *J. Appl. Phys.* **1998**, *83*, 4491.
[45] R. Asahi, T. Morikawa, T. Ohwaki, K. Aoki, Y. Taga, *Science* **2001**, *293*, 269.
[46] D. W. Wang, F. Li, J. P. Zhao, W. C. Ren, Z. G. Chen, J. Tan, Z. S. Wu, I. Gentle, G. Q. Lu, H. M. Cheng, *ACS Nano* **2009**, *3*, 1745.
[47] H. Q. Chen, M. B. Müller, K. J. Gilmore, G. G. Wallace, D. Li, *Adv. Mater.* **2008**, *20*, 3557.
[48] Z. H. Wang, L. Qie, L. X. Yuan, W. X. Zhang, X. L. Hu, Y. H. Huang, *Carbon* **2013**, *55*, 328.
[49] P. A. Nelson, J. R. Owen, *J. Electrochem. Soc.* **2003**, *150*, A1313.

[50] K. S. Park, A. Benayad, D. J. Kang, S.-G. Doo, *J. Am. Chem. Soc.* **2008**, *130*, 14930.
[51] Y. Shi, L. Wen, F. Li, H. M. Cheng, *J. Power Sources* **2011**, *196*, 8610.
[52] M. S. Song, A. Benayad, Y. M. Choi, K. S. Park, *Chem. Commun.* **2012**, *48*, 516.
[53] C. J. Kim, N. S. Norberg, C. T. Alexander, R. Kostecki, J. Cabana, *Adv. Funct. Mater.* **2013**, *23*, 1047.
[54] M. V. Reddy, T. Yu, C. H. Sow, Z. X. Shen, C. T. Lim, G. V. S. Rao, B. V. R. Chowdari, *Adv. Funct. Mater.* **2007**, *17*, 2792.
[55] T. Sasaki, M. Watanabe, H. Hashizume, H. Yamada, H. Nakazawa, *J. Am. Chem. Soc.* **1996**, *118*, 8329.
[56] G. Liu, L. Z. Wang, C. H. Sun, Z. G. Chen, X. X. Yan, L. N. Cheng, H. M. Cheng, G. Q. Lu, *Chem. Comm.* **2009**, 1383.
[57] Z. Qiu, L.Yang, Y. F. Tang, S. H. Fang, J. S. Huang, *Chin. J. Chem.* **2010**, *28*, 911.